Chinese Chemical Letters 31 (2020) 1044–1048

Contents lists available at ScienceDirect

Chinese Chemical Letters

journal homepage: www.elsevier.com/locate/cclet

Communication

From high-yield Ti_3AlCN ceramics to high-quality Ti_3CNT_x MXenes through eliminating Al segregation

Ningjun Chen[a], Haichao Huang[a], Zhong Xu[a], Yanting Xie[a], Da Xiong[a], Xiang Chu[a], Bingni Gu[a], Bo Zheng[a], Weili Deng[a], Haitao Zhang[a,*], Weiqing Yang[a,b,*]

[a] Key Laboratory of Advanced Technologies of Materials, Ministry of Education, School of Materials Science and Engineering, Southwest Jiaotong University, Chengdu 610031, China
[b] State Key Laboratory of Traction Power, Southwest Jiaotong University, Chengdu 610031, China

ARTICLE INFO

Article history:
Received 11 June 2019
Received in revised form 14 July 2019
Accepted 15 July 2019
Available online 14 October 2019

Keywords:
Al segregation
High-yield
Ti_3AlCN MAX phase
Ti_3CNT_x MXenes
Supercapacitors

ABSTRACT

Ti_3CNT_x MXenes with unique electrical conductivity can be widely applied for supercapacitors and electromagnetic shielding. However, its relatively low-yield quaternary nitrogen-containing Ti_3AlCN ceramics precursor (less than 50%), due to the inevitable Al segregation during the synthesizing process, significantly hindered its widely commercial applications. Herein, we employed the controllable AlN-oversaturation precursor strategy to precisely tune the phase transition point of quaternary Ti_3AlCN ceramics to obtain high-yield Ti_3AlCN precursor for the purpose of high conductivity Ti_3CNT_x MXenes. Combined energy dispersive X-ray spectrometer (XRD) with X-ray photoelectron spectroscopy (XPS) characterizations, the yield of the quaternary nitrogen-containing Ti_3AlCN ceramics was evidently proved to be up to 70%, which is 1.4 times than that of previously reported works. Such relatively high-yield quaternary Ti_3AlCN is mainly ascribed to the elimination of Al segregation. Based on it, we further developed accordion-like two-dimensional (2D) MXene *via* hydrofluoric acid etch and vacuum freeze-dry. This novel accordion-like 2D Ti_3CNT_x MXene possesses high electrochemical capacitive properties (209 F/g). Therefore, this controllable AlN-oversaturation precursor strategy will pave a way to exploit costly high-yield MAX ceramics precursor for high conductivity MXenes and also play a powerful role in promoting their practical applications including electrical and magnetic engineering fields.

MXenes, an etching derivative from insulated MAX ceramics, processes the unique electrical conductivity for the wide applications of supercapacitors and electromagnetic shielding, *etc*. [1–4]. While the high electronics performance of these new two-dimensional materials strongly depends on whether MAX ceramics precursor is good or bad as well as whether its yield is high or low. Therefore, it is a key to develop the high yield MAX ceramics. In this regard, the ternary-layered metal ceramic materials have recently attracted great attentions. Early in 1960s, V.H. Nowotny *et al.* successfully synthesized more than 30 carbon/nitrogen-containing compounds [5]. After that, M. Barsoum *et al.* renamed them as MAX phase, where M represents early transition metal elements such as Ti, V, Cr; A refers to the third or fourth main group, such as Al, Si, Ga, In, Sn, As, TI and Pb; X is C or N [6]. This unique MAX phase shows excellent properties such as high temperature resistance [7–9], elastic properties [10], phonon conductivities [10] and room-temperature electroconductivity [7]. Hence, they could be widely used in electrical mechanical, aerospace, medical engineering fields [11–15]. Among the MAX phase, Ti-Al-C systems such as Ti_3AlC_2 have been used as engine and heat exchanger materials due to their good plasticity and seismic resistance properties [16,17]. Except that, Ti_3SiC_2 has been also applied for the protective layers of nuclear reactor due to their radiation resistance properties [19,20].

The quaternary MAX usually has the more advantageous than ternary MAX in certain areas and certain occasions. On the one hand, the mechanical strength of recently-reported $Ti_3AlC_{2-x}N_x$ was proved to be enhanced with the increase of nitrogen content, which is by 20 GPa in Young's modulus higher than that of Ti_3AlC_2 [19]. On the other hand, Ti_3AlCN possesses higher conductivity than Ti_3AlC_2. After nitrogen substitution for carbon element endows the higher conductivity because of incorporating into the lone pair electrons from nitrogen element [20,21]. Therefore, this quaternary Ti_3AlCN would be an excellent precursor for

* Corresponding authors at: Key Laboratory of Advanced Technologies of Materials, Ministry of Education, School of Materials Science and Engineering, Southwest Jiaotong University, Chengdu 610031, China.
E-mail address: wqyang@swjtu.edu.cn (W. Yang).

https://doi.org/10.1016/j.cclet.2019.10.004
1001-8417/

further exploiting high conductivity Ti_3CNT_x MXenes. However, the variety of intermediate products causes the low yield of quaternary Ti_3AlCN MAX phase [14]. Previous work indicated that the yield of Ti_3AlCN was as low as only 50%, mainly ascribing to the reason that intermediate products such as TiN, TiC, Ti_2AlN and Ti_2AlC as a form of impurities present at the resultant samples [21,22]. Another reason is that the loss of nitrogen and aluminum elements, which leads to non-stoichiometry for Ti_3AlCN. At present, the common methods to improve the yield of MAX phase are adjusting the proportion and optimizing the sintering process [23]. However, there is still no effectively preparing method to produce high-yield quaternary nitrogen-containing MAX phase.

Similarly, compared with $Ti_3C_2T_x$, three layers titanium of Ti_3CNT_x MXene are sandwiched by both nitrogen and carbon layers instead of only carbon layers, making it possess unique properties. Recently, Qin *et al.* theoretically predicted that Ti_3CNT_x possesses high specific capacitance, and the electrochemical performance of 2D Ti_3CNT_x MXene is completely different from carbide based MXenes [15]. Therefore, synthetic Ti_3CNT_x MXene can promote the research of MXene in piezoelectric, diathermanous, light transmission, superconductive and biocompatible yields and so on. However, the capacitive properties of N-containing 2D Ti_3CNT_x MXene have not experimentally realized probably because the preparation of high-impurity Ti_3AlCN MAX precursor is difficult. Therefore, it is significant to explore an effective method to synthesize high-quality Ti_3AlCN MAX precursors.

In this work, we presented the adopted AlN-oversaturation precursor strategy to precisely tune the phase transition point of quaternary Ti_3AlCN ceramics to obtain high-yield Ti_3AlCN precursor for the purpose of high conductivity Ti_3CNT_x MXenes. The yield of this as-prepared quaternary Ti_3AlCN ceramics was as high as 70%, which is 1.4 times than that of previous reported works. Such high-yield quaternary Ti_3AlCN is mainly ascribed to the elimination of Al segregation. Based on it, we experimentally prepared accordion-like two-dimensional (2D) MXene via hydrofluoric acid etch and vacuum freeze-dry. This Ti_3CNT_x MXene shows the high electrochemical capacitive of 209 F/g. Therefore, this controllable AlN-oversaturation precursor strategy will potentially exploit costly high-yield MAX ceramics precursor for high conductivity MXenes and will also expand their practical applications including electrical and magnetic engineering fields.

The chemical is shown as follow, Titanium (99%, 300 mesh), aluminum nitride (99%, 300 mesh), and carbon black (99%, 2 μm) powders were purchased from Beijing Xing Rong Yuan Technology (China). Concentrated HF (40 wt%) was purchased from Chengdu Ke Long Co., Ltd. (China). All the chemicals were used without further purification.

The Ti_3AlCN powders were prepared by a solid-state sintering method. The powders titanium, aluminum nitride and carbon black with alcohol solvent were ball-milled respectively at molar ratios of 3:1:1, 3:1.2:1 and 3:1.4:1 for 12 h. For convenience, the Ti_3AlCN MAX powders were referred to as Ti_3AlCN-1.0, Ti_3AlCN-1.2 and Ti_3AlCN-1.4 accordingly. Afterwards, the mixtures were dried at room temperature for 24 h. For obtaining uniform particle size, the ball-milled mixtures were collected by screening from firstly 300 meshes and then to 400 meshes. Then, the mixtures were put into a corundum boat with a high-purity of 99.99% and further heated at 1500 °C in a tubular furnace at a ramping rate of 5 °C/min (GSL-1700X, Hefei Kejing Co., Ltd., China) under 40 sccm Ar flowing gas (GSL-2Z-LCD, Hefei Kejing Co., Ltd., China). Finally, the obtained bulk materials were drilled into powders and then sieved through a 300-mesh screen.

In order to prepare accordion-like Ti_3CNT_x MXene, we chose HF as the etchant to selectively remove the aluminum layers. For exfoliating, 1.2 g Ti_3AlCN powder was slowly added to HF (30 wt%), followed by stirring under 25 °C for 21 h. After that, the final suspension was repeatedly washed with enough DI water until the supernatant showing a pH value of 6.0. Finally, the resulted sediment was vacuum freeze-dried at −80 °C.

The characterizations are shown as follow: X-ray diffraction (XRD) patterns were obtained with a powder diffractometer (PANalytical X'Pert Powder diffractometer, Holland) using Cu Kα radiation with 0.02° 2θ steps. We used a scanning electron microscope, SEM (FEI QUANTA FEG 250, American) to obtain high-magnification images of Ti_3AlCN powder and freeze-dried powders of multilayered Ti_3AlCN MXene. Energy dispersive X-ray (EDX) spectroscopy was conducted in SEM (FEI QUANTA FEG 250, American). The chemical composition and surface terminations were detected *via* X-ray photoelectron spectroscopy (XPS) with a Thermo Scientific ESCALAB 250Xi spectrometer.

To clearly demonstrate the preparation of high-quality Ti_3AlCN MAX phase and its Ti_3CNT_x derivations, the metallographic Ti_3AlCN phases by adjusting the ratio of AlN are shown in Fig. 1a. Through eliminating the Al segregation, we obtained high-purity quaternary Ti_3AlCN phases. However, according to the stoichiometric molar ratio (Ti:Al:C:N = 3:1:1:1), the yield of Ti_3AlCN is only about 50% due to the loss of Al and N elements. Although Ti_3AlCN could stably exist in equilibrium according to the Ti-Al-C-N quaternary phase diagram, the intermediate products such as TiN, TiC, Ti_2AlN and Ti_2AlC could not be efficiently avoided, which determined that achieving high-purity Ti_3AlCN was very difficult [18,19]. Hence, herein reported incorporation of slightly excess AlN (the molar ratio is 1.2) is significant to prepare high-purity quaternary Ti_3AlCN phase. The slightly excess AlN compensates for the loss of Al and N elements since AlN is not thermal stability at high temperature [24,25]. Fig. 1b schematically gives the solid- state sintering and chemical etch process of the Ti_3AlCN and its Ti_3CNT_x MXenes. For increasing the yield of Ti_3AlCN, we add the excess AlN with the molar ratio ranging from 1.0 to 1.4. Exhilaratingly, we get a high yield of 70% for Ti_3AlCN samples when the molar ratio of AlN is 1.2. The appropriate excess AlN promoted the reversible reaction to a new equilibrium state by compensating the loss of Al and N elements. The reaction formulas are given as following:

$$3Ti + C + AlN \leftrightarrow \frac{1}{2}TiC + \frac{1}{2}TiN + \frac{1}{2}Ti_2AlC + \frac{1}{2}Ti_2AlN \quad (1)$$

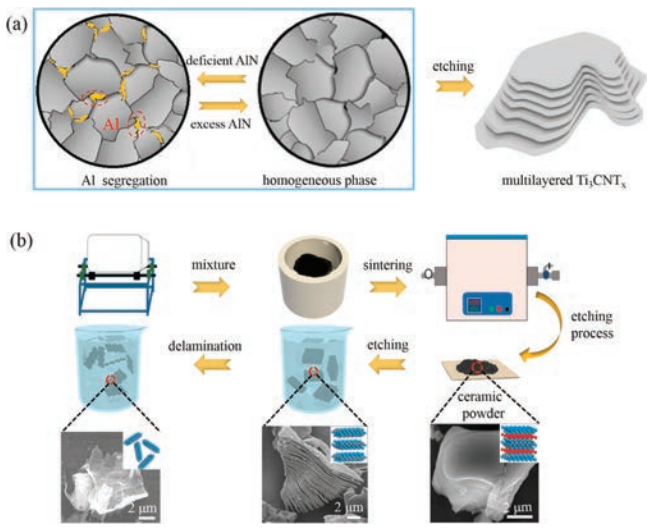

Fig. 1. Schematic illustration of metallographic and the synthetic route of Ti_3AlCN and Ti_3CNT_x samples. (a) Synthesis of high-purity Ti_3AlCN phase by adding excess AlN to eliminate Al segregation. And further synthesis of Ti_3CNT_x MXene by chemical etch and vacuum freeze-dry. (b) The detailed synthetic route, crystal structure and SEM micrographs of Ti_3AlCN and Ti_3CNT_x samples.

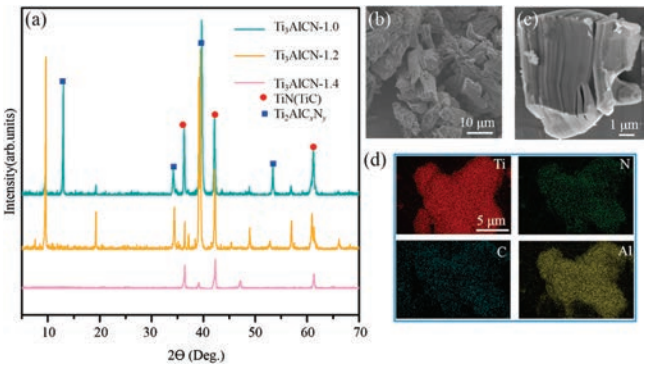

Fig. 2. Phase structure and compositions of the Ti_3AlCN samples. (a) Representative XRD patterns of Ti_3AlCN samples, and Ti_3AlC_2 are also given for comparing. (b) SEM image of Ti_3AlCN-1.2. (c) The enlarged SEM image of Ti_3AlCN-1.2. (d) EDX mapping of Ti_3AlC_2-1.2.

$$\frac{1}{2}TiC+\frac{1}{2}TiN+\frac{1}{2}Ti_2AlC+\frac{1}{2}Ti_2AlN\leftrightarrow Ti_3AlCN \quad (2)$$

However, sufficiently excess AlN (like a molar ratio of 1.4) can cause the reaction to end at the stage where the formation energy of result is low because the decomposition of AlN is an endothermic reaction [26]. SEM images and the crystal structures of Ti_3AlCN MAX phase, the accordion-like Ti_3CNT_x MXene and single-layer Ti_3CNT_x are shown in the bottom of Fig. 1b.

The XRD patterns of Ti_3AlCN ceramic powder samples are shown in Fig. 2a. Comparatively, Ti_3AlCN-1.0 was prepared according to the stoichiometric molar ratio (Ti:Al:C:N = 3:1:1:1). However, the Ti_3AlCN yield contains many impurities including TiN/TiC, and $Ti_2AlC_xN_y$. As the molar ratio of AlN increases to 1.2, the contents of the impurities become less. The reason is that the appropriate more AlN can compensate for lost Al and N element and promote the reversible reaction to a new equilibrium state [20]. However, the TiN/TiC, and $Ti_2AlC_xN_y$ impurities are still presented while the main phase of Ti_3AlCN reaches up to 70%, which is much higher than previously reported work [20]. As the molar ratio of AlN increased to 1.4, Ti_2AlC and TiN phases instead of Ti_3AlCN were prepared since excess AlN caused the reaction to end at the stage where the formation energy is the lowest [27]. Obviously, increasing the amount of AlN moderately does increase the yield of Ti_3AlCN due to elimination of Al segregation *via* adjusting the AlN composition, however, this procedure needs to be carefully controlled.

For a further characterization of Ti_3AlCN-1.2 MAX phase, SEM measurements were performed on Ti_3AlCN-1.2 MAX powder. Figs. 2b and c are low and high magnification images, respectively. MAX phase presented a distinct ladder-like morphology, indicating its layer-like crystal structure in nature. Simultaneously, it also implies that the growth rate along the c-axis is greater than that in a-axis [2,3]. According to EDX analysis (Fig. 2d), Ti, N, C and Al elements in Ti_3AlCN-1.2 are uniformly distributed. For comparing, the atomic ratio, the SEM images and EDX of Ti_3AlCN-1.0 and Ti_3AlCN-1.4 samples were also shown (Figs. S1 and S2 in Supporting information).

We performed XPS measurements to further identify the composition and chemical bonding information of the Ti_3AlCN MAX phase. In Fig. 3, XPS full-scan spectra and deconvolution XPS spectra of Ti_3AlCN-1.2 samples are illustrated. Figs. 3b-f are Al 2p, N 1s, O 1s, Ti 2p and C 1s, respectively. As shown in the Al 2p spectra (Fig. 3b), the peaks were fitted to Al—C, Al—Ti and Al—N, bonds. Fig. 3c shows XPS spectra in the N 1s region that corresponds to N—Ti, N—C, Al-N. Accordingly, O—Ti, O—C and O—Al groups are found in the O 1s high-resolution spectrum. The Ti 2p spectrum (Fig. 3e) was fitted by components corresponding to Ti—C, Ti—Al, Ti—N, Ti—O. The binding energies (B.E.) of the Ti—N species shifts to higher B.E. of 460.8 eV in comparison with Ti—C species that is 454.4 eV, and a part of the N atom exists as TiN compound. Fig. 3f plots high-resolution spectrum in the C 1s region that was fitted by components corresponding to the following species: C—C, C—Ti, C–N and C–O. Finally, the ratio of C atom to N atom involving in the formation of Ti_3AlCN is basically equal to 1:1 by calculation. In a word, high-purity Ti_3AlCN was successfully prepared by simply adjusting the AlN composition and about 50% carbon atoms were replaced by nitrogen atoms that accords to the stoichiometric proportion of Ti_3AlCN.

$Ti_3C_2T_x$ MXene was proved to possess excellent electrochemical performance than most of the other MXenes. Incorporation of N into $Ti_3C_2T_x$ brings about high conductivity and much more

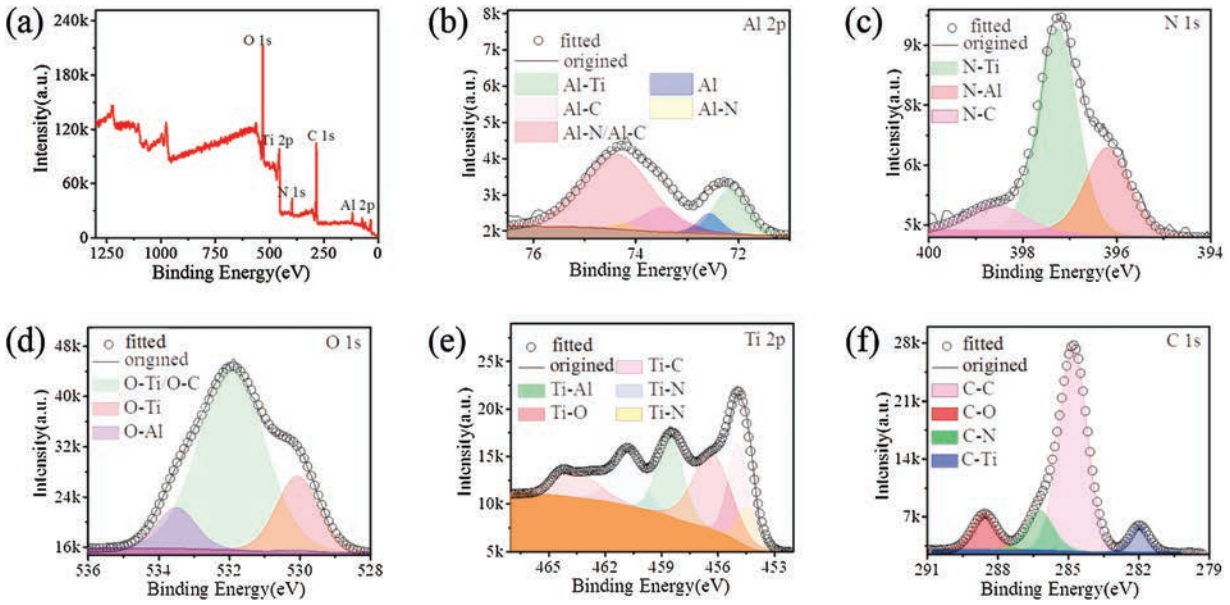

Fig. 3. XPS spectra of the Ti_3AlCN MAX phase. (a) XPS full spectrum of the freeze-dried sample. High-resolution XPS spectra of (b) Al 2p, (c) N 1s, (d) O 1s, (e) Ti 2p and (f) C 1s.

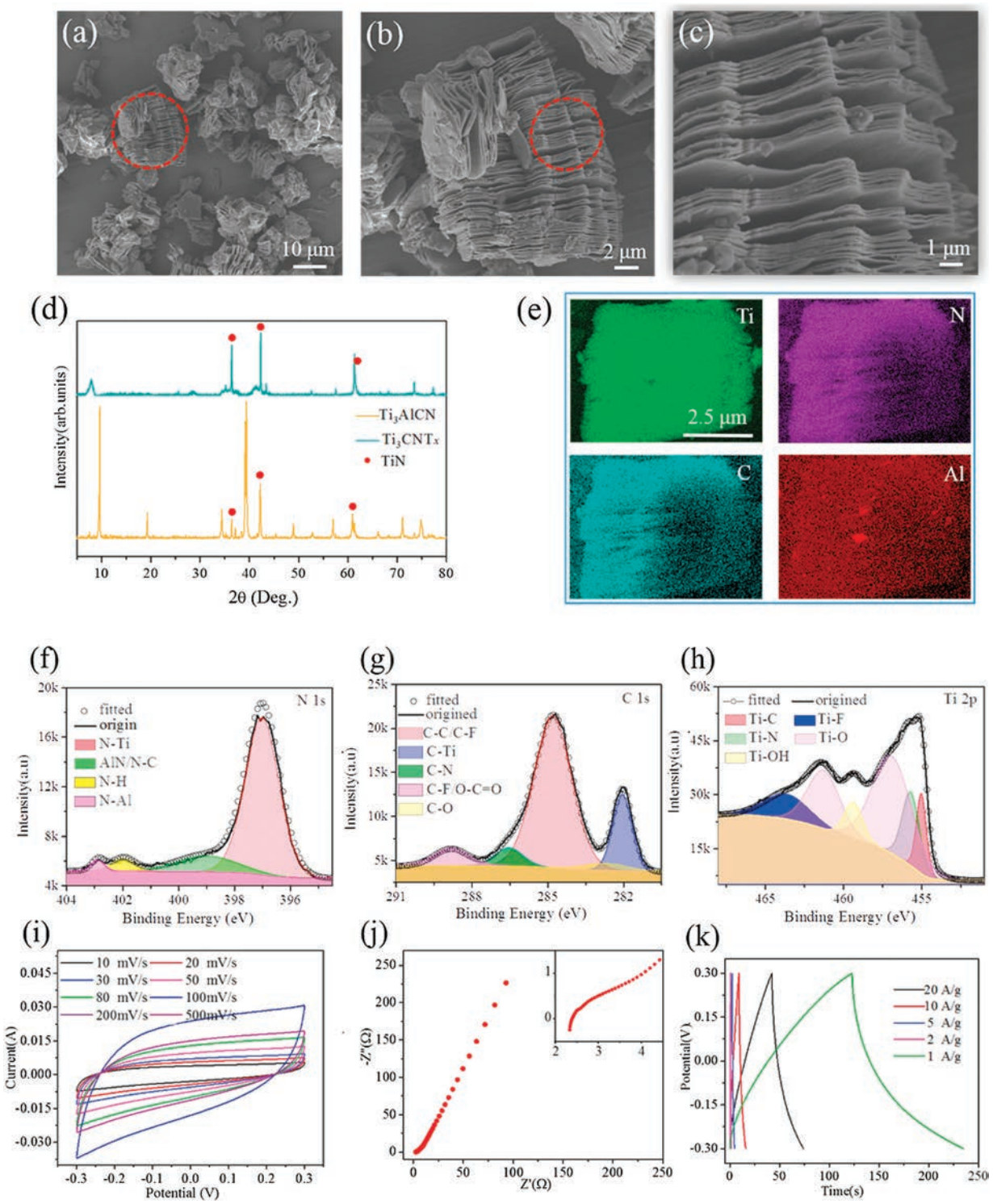

Fig. 4. Morphology, phase structure and compositions of the Ti_3CNT_x samples. (a-c) FESEM of accordion-like Ti_3CNT_x samples. (d) XRD patterns of accordion-like Ti_3CNT_x samples. XRD pattern of Ti_3AlCN-1.2 precursor is also given for comparing. (e) EDX mapping of Ti_3CNT_x. The compositions of accordion-like multilayered Ti_3CNT_x. Deconvoluted XPS spectra of (f) N 1s, (g) C 1s, and (h) Ti 2p. (i) CV curves at the scan rates varying from 10 mV/s to 500 mV/s. (j) Electrochemical impedance spectroscopy of Ti_3CNT_x Films. (k) GCD curves at different charge-discharge current densities.

electrochemically active sites that probably make Ti_3CNT_x possess high specific capacitance in theoretically. Hence, we prepared accordion-like 2D Ti_3CNT_x MXene through chemical etch and vacuum freeze-dry. As shown in Figs. 4a-c, the freeze-dried Ti_3CNT_x powder maintains platelet shape at different magnifications. The bond energy of Ti—C and Ti—N bonds are mainly covalent bonds, which is stronger than Ti—Al. Hence, Al atoms can be firstly removed from the layered structure [28,29]. As the Al atomics are completely stripped, ladder-like MAX particles transform into 2D accordion- like MXenes [22]. Fig. 4e shows the elemental mapping (EDX) corresponding to accordion-like 2D Ti_3CNT_x MXene. Apparently, Ti, C and N elements in accordion-like

2D Ti_3CNT_x MXene are evenly distributed. After etching, the main force between the sheets is van der Waals force and hydrogen bond. The XRD patterns of Ti_3CNT_x-1.2 were shown in Fig. 4d. Compared with MAX phase, the interlay spacing between the layers increases as indicated by XRD results, mainly ascribing to the selective etch of Al elements. In addition, the freeze-dried powder has a considerable amount of impurity phase, TiN because HF cannot remove it.

For further identifying the composition and chemical bonding of the accordion-like Ti_3CNT_x, XPS measurements were performed. In Figs. 4f-h, XPS full-scan spectra and deconvoluted XPS spectra of freeze-dried sample are illustrated. The total elemental composition of the accordion-like 2D Ti_3CNT_x MXene shows the present of titanium, nitrogen, carbon, oxygen, fluorine, and aluminum in the expected amounts (Fig. S3a in Supporting information). Figs. 4f-h are N 1s, C 1s and Ti 2p, respectively. As shown in the C 1s spectra (Fig. 4g), the peaks were fitted to C—C/C—F, C—Ti, C–N, COO and C–O bonds. The Ti 2p spectrum (Fig. 4h) was fitted by components corresponding to bonds: Ti—C, Ti—F, Ti—N, Ti—O, Ti—OH, indicating the multilayered Ti_3CNT_x were terminated by surface functionalities such as —OH, —F and —O, *etc*. The relative quantity of Ti—O in the Ti_3CNT_x is more than that in the $Ti_3C_2T_x$. Fig. 4f shows XPS spectra in the N 1s region that corresponds to N—Ti, N—C/Al-N and N—H [30–32]. Distinctly, the impurity phase TiN took up vast N-bond. The ratio of C: N equals to 1:1 by computing XPS data. As shown in the Fig. 4h, Ti—C peaks centering at 455.2 eV, the Ti-N bonds are stronger than Ti—C bonds that the BE of them correspond to 456.3 eV. Accordingly, F—C, F—Ti and F—Al are found in the F 1s high-resolution spectrum (Fig. S3b in Supporting information), and O—H, O—C, H_2O, O=C, O—Ti groups are found in the O 1s high-resolution spectrum (Fig. S3c in Supporting information). Therefore, MXene sheet were intercalated by many functional groups such as –O, —OH and –F. Moreover, the capacitive performance of Ti_3CNT_x films, assisted synthesized with binder (10 wt% polyvinylidene fluoride), is shown in Figs. 4i-k. The Ti_3CNT_x films were tested by cyclic voltammetry (CV) at various scan rates ranging from 10 mV/s to 500 mV/s (Fig. 4i). As a result, these Ti_3CNT_x films show nearly rectangular CV profiles up to 500 mV/s, indicating excellent cycle stability and rapid response time. The ohmic resistance (the sum of intrinsic material resistance, electrolyte resistance and the contact resistance between collector with intrinsic material) is less than 2.2 Ω, indicated in Fig. 4j. Specially, many -F surface functionalities and polymer binder caused slightly higher resistance than that of Ti_3CNT_x MXenes films without polymer binder. From Fig. 4k, the special capacitance is up to 209 F/g at a current density of 1 A/g.

In conclusion, we presented the controllable AlN-oversaturation precursor strategy to successfully tune the phase transition point of quaternary Ti_3AlCN ceramics to obtain high-quality Ti_3AlCN precursor for the purpose of high conductivity Ti_3CNT_x MXenes. Due to the elimination of Al segregation, the yield of as-prepared quaternary nitrogen-containing Ti_3AlCN ceramics was up to 70%, which is higher than that of previous reported works. Based on it, we developed accordion-like two-dimensional (2D) MXene. This 2D Ti_3CNT_x MXene has high electrochemical capacitive properties of 209 F/g. Therefore, we believe that this controllable AlN-oversaturation precursor strategy would open a way to exploit costly high-yield MAX ceramics precursor for high conductivity MXenes and also substantially promote their practical applications including electrical and magnetic engineering fields.

Declaration of competing interest

The authors declare that they have no known competing financial interests or personal relationships that could have appeared to influence the work reported in this paper.

Acknowledgments

We are thankful to Analytical and Testing Center of Southwest Jiaotong University for supporting the SEM measurements. This work is supported by the National Natural Science Foundation of China (No. 51602265), the Special Fund of China Postdoctoral Science Foundation (No. 2018T110992), the Sichuan Science and Technology Program (No. 2018RZ0074) as well as the Cultivation Program for the Excellent Doctoral Dissertation of Southwest Jiaotong University (No. D-YB201709).

Appendix A. Supplementary data

Supplementary material related to this article can be found, in the online version, at doi:https://doi.org/10.1016/j.cclet.2019.10.004.

References

[1] N. Kurra, B. Ahmed, Y. Gogotsi, H.N. Alshareef, Adv. Energy Mater. 6 (2016) 1601372.
[2] R. Sun, H.B. Zhang, J. Liu, et al., Adv. Funct. Mater. 27 (2017) 1702807.
[3] L. Feng, K. Wang, X. Zhang, et al., Adv. Funct. Mater. 28 (2018) 1704463.
[4] X. Zhao, C. Li, X. Zhang, et al., ChemistrySelect 2 (2017) 6194–6199.
[5] V.H. Nowotny, Prog. Solid State Chem. 5 (1971) 27–70.
[6] N.V. Tzenov, M.W. Barsoum, J. Am. Ceram. Soc. 83 (2010) 825–832.
[7] T.H. Scabarozi, S. Amini, P. Finkel, et al., J. Appl. Phys. 104 (2008) 201.
[8] P. Yu, G. Cao, S. Yi, et al., Nanoscale 10 (2018) 5906–5913.
[9] M. Xu, N. Bai, H. Li, et al., Chin. Chem. Lett. 29 (2018) 1313–1316.
[10] M. Radovic, A. Ganguly, M.W. Barsoum, J. Mater. Res. 23 (2008) 1517–1521.
[11] M.A. Borysiewicz, E. Kamińska, A. Piotrowska, I. Pasternak, R. Jakieła, Acta Phys. Pol. A 114 (2008) 1061–1066.
[12] E.N. Hoffman, D.W. Vinson, R.L. Sindelar, et al., Nucl. Eng. Des. 244 (2012) 17–24.
[13] H. Su, H. Huang, H. Zhang, et al., ACS Appl. Energy Mater. 1 (2018) 3544–3553.
[14] H. Zhang, H. Su, L. Zhang, et al., J. Power Sources 331 (2016) 332–339.
[15] X. Chu, H. Zhang, H. Su, et al., Chem. Eng. J. 349 (2018) 168–175.
[16] M.A. Pietzka, J.C. Schuster, J. Am. Ceram. Soc. 79 (1996) 2321–2330.
[17] B. Velasco, E. Gordo, L. Hu, M. Radovic, S.A. Tsipas, J. Alloys. Compd. 764 (2018) 24–35.
[18] H. Zhang, R. Su, L. Shi, et al., Appl. Surf. Sci. 434 (2018) 1210–1216.
[19] X. Qin, P. Zhang, S. Wang, et al., Phys. Status Solidi B 254 (2017) 1700009.
[20] N. Haddad, E. Garcia-Caurel, L. Hultman, M.W. Barsoum, G. Hug, J. Appl. Phys. 104 (2008) 023531.
[21] F. Du, H. Tang, L. Pan, et al., Electrochim. Acta 235 (2017) 690–699.
[22] M. Naguib, O. Mashtalir, J. Carle, et al., ACS Nano 6 (2012) 1322–1331.
[23] J. Guo, K. Chen, H. Zhou, X. Ning, Acta Mater. Compositae Sin. 32 (2003) 561–565.
[24] F.C. Sauls, W.J.H. Jr, L.V. Interrante, P.S. Marchetti, G.E. Maciel, Chem. Mater. 7 (1995) 1361–1368.
[25] R. Grieseler, T. Kups, M. Wilke, M. Hopfeld, P. Schaaf, Mater. Lett. 82 (2012) 74–77.
[26] J. Lis, R. Pampuch, T. Rudnik, Z. Węgrzyn, Solid State Ion. 101 (1997) 59–64.
[27] B. Manoun, S.K. Saxena, G. Hug, et al., J. Appl. Phys. 101 (2007) 113523.
[28] G. Ying, A.D. Dillon, A.T. Fafarman, M.W. Barsoum, J. Mater. Res. Lett. 9439 (2017) 1–8.
[29] H. Huang, H. Su, H. Zhang, et al., Adv. Electron. Mater. 4 (2018) 1800179.
[30] J. Halima, K.M. Cook, M. Naguibe, et al., Appl. Surf. Sci. 362 (2016) 406–417.
[31] B. Soundiraraju, B.K. George, ACS Nano 11 (2017) 8892–8900.
[32] H. Wang, J. Zhang, Y. Wu, et al., Appl. Surface Sci. 384 (2016) 287–293.